Journal of Magnetism and Magnetic Materials 354 (2014) 178–183

Contents lists available at ScienceDirect

Journal of Magnetism and Magnetic Materials

journal homepage: www.elsevier.com/locate/jmmm

Structural analysis and magnetic properties of solid solutions of Co–Cr system obtained by mechanical alloying

J.A. Betancourt-Cantera [a], F. Sánchez-De Jesús [a,*], A.M. Bolarín-Miró [a], I. Betancourt [b], G. Torres-Villaseñor [b]

[a] Área Académica de Ciencias de la Tierra y Materiales, UAEH Carr., Pachuca-Tulancingo Km. 4.5, Pachuca, Hidalgo 42184, Mexico
[b] Departamento de Materiales Metálicos y Cerámicos, Instituto de Investigaciones en Materiales, Universidad Nacional Autónoma de México, México D.F. 04510, Mexico

ARTICLE INFO

Article history:
Received 11 December 2012
Received in revised form
16 October 2013
Available online 7 November 2013

Keywords:
Mechanical alloying
Co–Cr system
Saturation polarization
Coercive field
Curie temperature

ABSTRACT

In this paper, a systematic study on the structural and magnetic properties of $Co_{100-x}Cr_x$ alloys ($0 < x < 100$, $\Delta x = 10$) obtained by mechanical alloying is presented. Co and Cr elemental powders were used as precursors, and mixed in an adequate weight ratio to obtain $Co_{1-x}Cr_x$ ($0 < x < 100$, $\Delta x = 10$). Mechanical milling was carried out at room temperature in a shaker mixer mill using vials and balls of hardened steel as the milling media with a ball:powder weight ratio of 10:1. The mixtures were milled for 7 h. Results shown that after 7 h of milling time, solid solutions based on Co-hcp, Co-fcc and Cr-bcc structures were obtained. The saturation polarization indicated a maximum value of 1.17 T (144 Am^2/kg) for the $Co_{90}Cr_{10}$, which decreases with the increasing of the Cr content up to $x = 80$, as a consequence of the dilution effect of the magnetic moment which is caused by the Cr content and by the competition between ferromagnetic and antiferromagnetic exchange interactions. The coercivity increases up to 34 kA/m (435 Oe) for $Co_{40}Cr_{60}$. For Cr rich compositions, it is observed an important decrease reaching 21 kA/m (272 Oe) for $Co_{10}Cr_{90}$, it is related to the grain size and the structural change. Besides, the magnetic anisotropy constant was determined for each composition. Magnetic thermogravimetric analysis allowed to obtain Curie temperatures corresponding to the formation of hcp-Co(Cr) and fcc-Co(Cr) solid solutions.

1. Introduction

Cobalt-based alloys have been in use since 1907 when Elwood Haynes obtained the first patent on cobalt–chromium compositions [1]. Following this patent, Co–Cr alloys have been of great importance because of their excellent mechanical properties such as wear and corrosion resistance, along with their excellent biocompatibility which permits their use in biomedical devices such as dental and surgical implants [2]. Co–Cr alloys are also the base composition for many steels, high temperature alloys, and magnetic materials [3]. As thin films, these alloys are widely used as magnetic recording media in computer hard discs [4]. Pure cobalt has an hcp crystal structure (ε-cobalt) at room temperature that transforms to the fcc structure (α-cobalt) upon heating at 673 K. The wear resistance of cobalt alloys is partially due to a structural transformation that these alloys undergo during mechanical deformation. This transformation can be explained in terms of the metastability of the Co-fcc phase at room temperature which becomes unstable when an external mechanical force or thermal energy is introduced [5]. In addition, this transformation depends upon alloying elements, such as chromium, molybdenum, and tungsten, that increase the transformation temperature and therefore enhance the stability of the hcp structure [6], whereas elements such as nickel and iron suppress the transformation temperature, yielding stable fcc structures [6,7].

Mechanical alloying (MA) is a material synthesis method that creates a large number of crystal defects and stacking faults due to the severe plastic deformation that results from the high energy supplied to the system [8,9]. This enables structural changes such as allotropic transformations [10–19] that normally only occur at high temperatures [14]. In addition, the magnetic properties of mechanically alloyed materials can be notably influenced by the MA process due to the stresses and defects that are generated during the milling process, together with a consequent grain size reduction that results in an increase of the magnetization and coercivity [20,21]. The aim of this work is to present a systematic study of the crystal structure and magnetic properties of the $Co_{100-x}Cr_x$ alloy system with $10 \leq x \leq 90$ and $\Delta x = 10$ synthesized by mechanical alloying, MA.

2. Experimental details

Elemental cobalt powder (Sigma-Aldrich, >99.9%), with a mean particle size (D_{50}) of 10 μm and elemental chromium

* Corresponding author. Tel.: +52 771 716 3932.
E-mail addresses: fsanchez@uaeh.edu.mx, zeppelin52004@yahoo.com.mx (F. Sánchez-De Jesús).

0304-8853/$ - see front matter © 2013 Elsevier B.V. All rights reserved.
http://dx.doi.org/10.1016/j.jmmm.2013.10.042

powder (Sigma-Aldrich, > 99.9%) with a mean particle size (D_{50}) of 30 μm were used as precursors. The elemental powders (Co and Cr) were mixed in the appropriate weight ratio to obtain $Co_{100-x}Cr_x$ alloys, where x varies from 10 to 90 with $\Delta x = 10$. A total amount of 5 g of the starting mixtures together with 6 hardened steel balls of 12.7 in diameter mm were loaded into a steel vial with 64.6 cm^3 of volume and milled for 7 h in a high energy ball miller. Hardened steel balls were used as milling media because in several works it have demonstrated that provide enough energy to promote solid state transformation during high energy ball mill in metallic systems [8–24].

The milling process was carried on at room temperature in argon atmosphere using a SPEX 8000D shaker mill. The ball-to-powder weight ratio was 10:1. To prevent excessive overheating of the vials, all experiments were performed using cycles of 90 min of milling followed by 20 min of rest, until achieving 420 min (7 h) of milling time.

The milled powders for different compositions ($Co_{100-x}Cr_x$) were characterized by X-ray diffraction (XRD) using a Siemens D5000 diffractometer, in order to know the phase transformations as a function of the composition and milling time. The diffraction parameters were collected with 2θ ranging from 35° to 120° with a step size of 0.02 and Co K_α ($\lambda = 1.7889$ Å) radiation. Morphological characterization was performed using a Leica Stereoscan 440 electron microscope operated at 20 kV. The magnetic properties of the milled powders, specifically the saturation polarization (J_S) and coercivity (H_C), were obtained from magnetic hysteresis curves, using a LDJ9600 vibrating magnetometer (VSM) with a maximum applied field of 1.2 MA/m (15 kOe). The magnetic measurements were made on compacted powders at 6.5 g/cm^3 of green density; these compacts were prepared using 0.2 g of each milled powder and pressed into a cylindrical die of 5 mm in diameter. The magnetocrystalline anisotropy was calculated using the collected data from magnetic hysteresis loop, such as is described in the results. In addition, the Curie temperature of the alloys was determined using the magnetic thermogravimetric technique on a TGA/SDTA 851e Mettler-Toledo. These experiments were performed under argon atmosphere at temperatures in the range from 600 K to 1500 K.

3. Results and discussion

3.1. Structural analysis

Fig. 1 shows the XRD patterns of $Co_{100-x}Cr_x$ ($10 < x < 90$, $\Delta x = 10$), as a function of the chromium content (x, percentage in weight) milled for 7 h. The XRD patterns of the elemental powders, Co and Cr without milling ($x = 0$ and 100% respectively), also presented in this figure, confirm the presence of cobalt with two phases (Co-hcp and Co-fcc) and chromium with one phase (Cr-bcc). After 7 h of milling time for the $Co_{90}Cr_{10}$ alloy, the diffusion of Cr into the Co structure has led to the formation of Co(Cr) solid solution, and for this reason, no Cr-bcc reflection peaks are observed in the XDR pattern for this composition. In the XRD of $Co_{90}Cr_{10}$ it can be observed the reflection peaks corresponding to fcc-Co phase. Besides, it is evident that the allotropic transformation of Co from hcp to fcc has partially occurred, due to the unique peak of the fcc phase, that does not overlap with any hcp peak, has diminished. The presence of hcp-Co phase can be clearly seen in elemental Co ($x = 0$) confirmed by the presence of the reflection (1 0 2) and (1 0 3) peaks. It is know that this allotropic transformation occurs when the cobalt is subjected to an external mechanical or thermal energy, as a consequence of the accumulation of stacking faults induced during the mechanical milling [9–22]. For this composition a mixture of fcc and hcp is present.

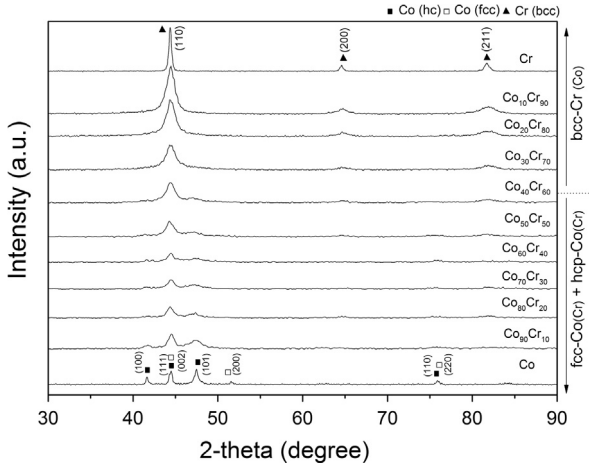

Fig. 1. XRD patterns for $Co_{100-x}Cr_x$ ($10 < x < 90$, $\Delta x = 10$) milled for 7 h.

Similar behavior is observed for $Co_{80}Cr_{20}$, where Cr peaks have vanished and only it can be observed reflection planes corresponding to a mixture of Co-fcc and Co-hcp phases. However, plane (2 0 0) of the fcc phase appears clearer in this composition, which confirms the preponderance of Co(Cr) with fcc structure. Same case is observed for compositions with x from 0 to 60, in these cases there is a mixture of allotropic phases of Co-fcc and Co-hcp where Cr is inside of both Co structures.

For $Co_{30}Cr_{70}$, it can be observed that reflection peaks that belong to cobalt disappear completely, and only peaks corresponding to bcc chromium are observed. This suggests a complete diffusion of cobalt atoms into the chromium structure and thus the formation of the Cr(Co) solid solution with bcc phase. The same behavior is observed for $Co_{20}Cr_{80}$ and $Co_{10}Cr_{90}$, accompanied by a diminution in the broadening of peaks, which is related to the refinement of the microstructure and the presence of microstrain caused by the introduction of the crystal defects during the mechanical alloying. In this case, the increase of the relative intensity of the peaks is due to the increase of the chromium content.

Besides, the crystal size for each composition was calculated using the Williamson-Hall method, following:

$$B_s \cos\theta = 2\varepsilon \sin\theta + \frac{K\lambda}{D} \quad (1)$$

where B_s is the full-width at half the maximum of the diffraction peak, θ is the Bragg angle, ε is the internal microstrain, λ is the wavelength of the X-ray, D is the crystallite size, K is a constant. B_s can be given as $B_s^2 = B_m^2 - B_c^2$. Where B_s is the width at half the maximum of the silicon powder peak used for calibration and B_m is the evaluated width. In this method $B_s \cos\theta$ is plotted against $2\sin\theta$, ε is the slope and $K\lambda/D$ is the interception [23].

The outcome of the evaluation of crystal size is shown in Fig. 2. In this Figure it is observed a progressive decrease of the crystallite size from 34.49 nm to 10.17 nm for 10 and 70 in wt. of Cr respectively, confirming the stabilization of the Co-fcc phase, where Cr atoms are packet in fcc structure increasing the atomic packing factor (APF), and helping to induce a diminution in the lattice parameters, and also, to produce severe plastic deformations together with accumulation of large amount of structural defects during the milling process. For compositions higher than 70 in wt. of Cr, it is observed an increase of the crystal size, up to 28.89 nm for 90 in wt. of Cr, this can be associated to the presence of Cr-bcc phase and the incorporation of a smaller atom, such as substituting atoms of Co (metallic radii 1.25 Å) for Cr (metallic radii 1.29 Å) into the Cr-bcc (*Pm*-3*m* structure)., whereas the

observed increase at the end of the compositional series is attributed to a major dislocation generation caused by severe plastic deformation and related to the formation of the bcc-Cr(Co) solid solutions.

3.2. Morphology and particle size analysis

Fig. 3 shows SEM micrographs that illustrate the morphology of the milled powder for the selected compositions. Due to the repeated fracturing, cold welding, and agglomeration of the powders during the mechanical alloying, a noticeable change in the shape and size of the samples is obtained. Lamellar type morphology is observed for x content between 10 and 50 due to the plastic deformation induced during the milling process (micrographics a) and b). For these compositions, the particles of Cr are fractured and joined into the lamellar particles. Therefore, high cobalt contents promote the formation of large agglomerates.

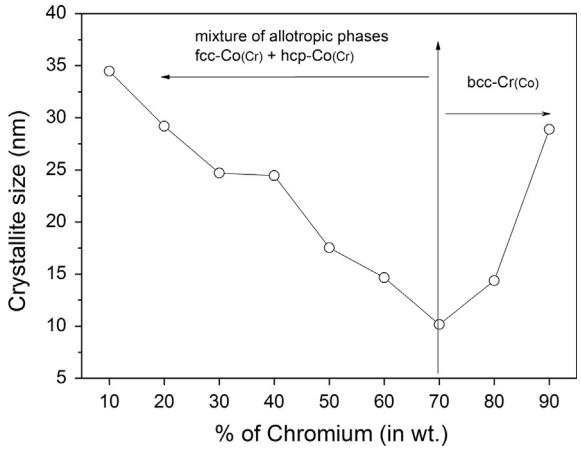

Fig. 2. Crystallite size and microstrain as a function of Cr content for the $Co_{100-x}Cr_x$ ($10 < x < 90$, $\Delta x = 10$) milled for 7 h.

On the other hand, the increase of Cr content (> 50% in wt.) promotes a decrease in the particle size. In this case, the reduction of the particle sizes is a result of the marked brittleness of chromium which does not permit sufficient plastic deformations [9]. In addition, possible iron contamination from the milling medium was examined using the EDX technique for all samples. No elemental iron was observed for compositions up to 50 in wt% of Cr, whereas for Cr rich base alloys, small amounts of iron were detected for each composition, around 0.5 in wt. ± 0.05. This effect of increase of iron with increasing of Cr is due to the lower ductility of the alloys, reducing their ability of adhesion and coating of the milling media and the containers, leading to wear and the contamination of alloys with iron.

The particle size was also measured using laser light diffraction. Results about the mean diameter are reported in Table 1. A considerable decrease in particle size with the increment of Cr is

Table 1
Particle size (mean diameter) for the $Co_{100-x}Cr_x$ alloy.

x (Cr wt%)	$D_{m50} \pm \sigma$(μm)
10	50.1 ± 0.42
20	33.0 ± 0.41
30	28.2 ± 0.36
40	24.3 ± 0.27
50	22.8 ± 0.37
60	19.8 ± 0.29
70	9.7 ± 0.16
80	9.3 ± 0.17
90	6.6 ± 0.36

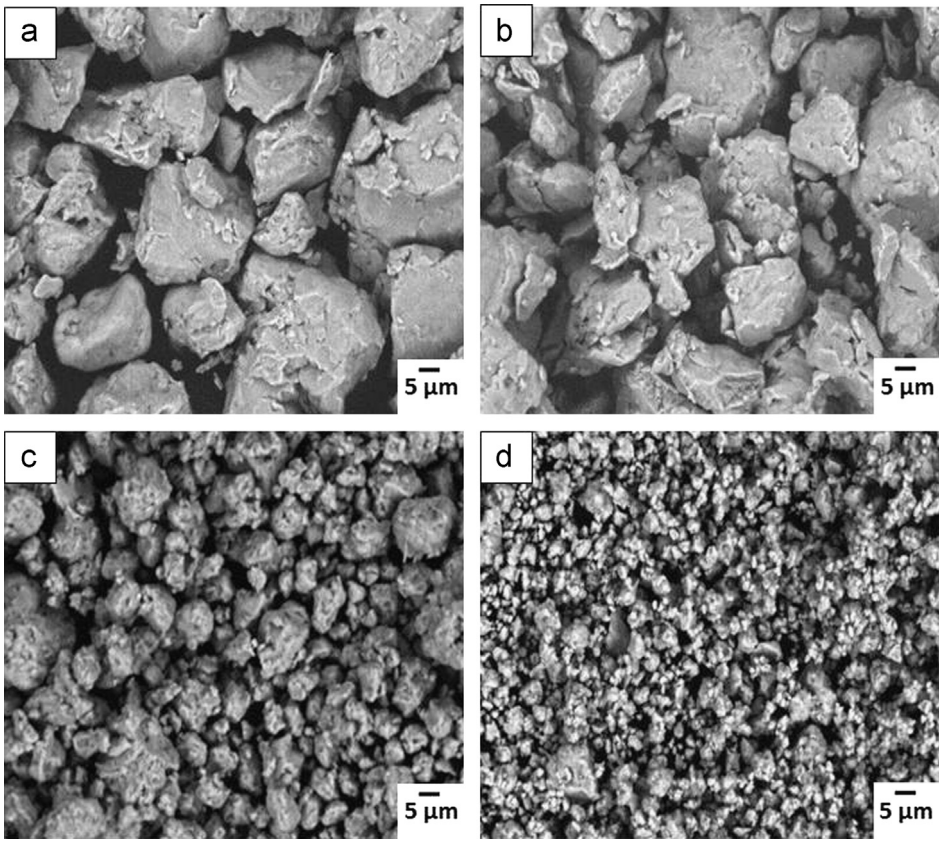

Fig. 3. SEM micrographs for different compositions: (a) $Co_{90}Cr_{10}$, (b) $Co_{60}Cr_{40}$, (c) $Co_{30}Cr_{70}$ and (d) $Co_{10}Cr_{90}$.

observed, from 50.12 μm to 6.65 μm for $Co_{90}Cr_{10}$ and $Co_{10}Cr_{90}$, respectively. The reduction in particle size is induced by the increase of chromium content, and by the fracturing forces that are developed during the MA process, due to the chromium is a brittle material. The particle sizes presented in Table 1 are in good agreement with the micrographs showed in Fig. 3.

3.3. Magnetic properties

Fig. 4 shows the magnetic hysteresis loops (*J–H*) for $Co_{100-x}Cr_x$ alloys ($10 < x < 90$). Here is remarkable that all the compositions show a weak behavior as a ferromagnetic material, with low coercivity and high saturation polarization. Also, a significant increase in saturation polarization is observed respect to the same compositions only mixed, confirming a solid solution formation between pure elements (Co and Cr) after the milling process.

Fig. 5 presents the magnetic parameters obtained from the *J–H* loops: saturation polarization, J_S, and coercivity, H_C. As can be observed in this figure, the J_S decreases drastically with the increase of the chromium content. The minimum value was obtained for $Co_{20}Cr_{80}$, as shown in Fig. 5. Besides, the J_S decreases from 1.17 T (144.1 Am^2/kg) for $Co_{90}Cr_{10}$ to 0.025 T (3.1 Am^2/kg) for $Co_{20}Cr_{80}$. This noticeable decrease of J_S can be attributed to the dilution effect of the magnetic moment of cobalt atoms promoted by the formation of the Co(Cr) and Cr(Co) solid solutions (structural change). Also, the increase of the chromium content promotes competition between ferromagnetic and antiferromagnetic exchange interactions [24]. Because of this, the J_S diminishes, also due to the increase of the antiferromagnetic exchange interactions and the decrease of the ferromagnetic exchange interactions. For the $Co_{30}Cr_{70}$ and $Co_{10}Cr_{90}$, the J_S exhibits a slight increment respect to $Co_{20}Cr_{80}$ around 0.004 T (1.2 Am^2/kg). This behavior can be attributed to the presence of iron as contamination from the synthesis method, as mentioned before.

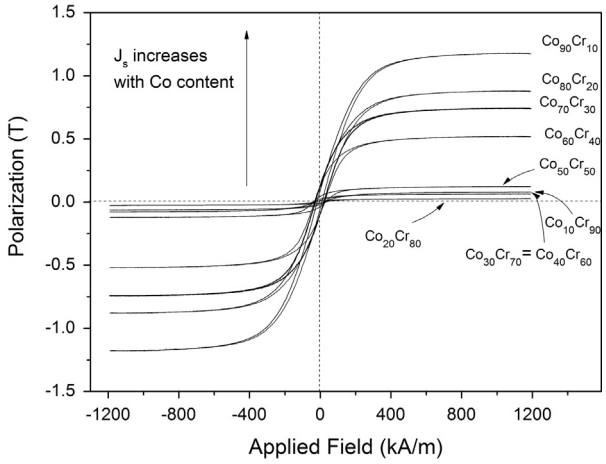

Fig. 4. Magnetic hysteresis loops (*J–H*) for $Co_{100-x}Cr_x$ ($10 < x < 90$, $\Delta x = 10$) milled for 7 h.

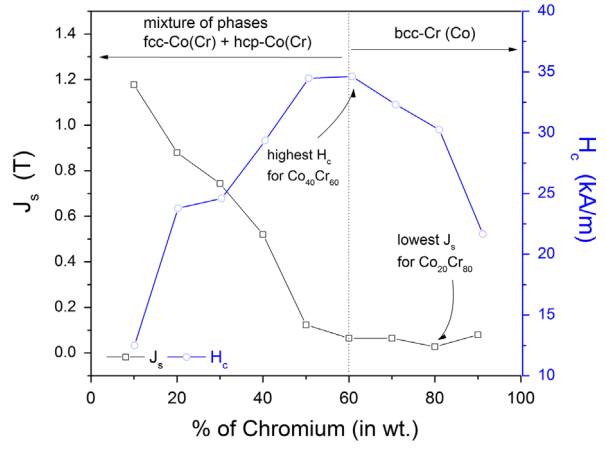

Fig. 5. Saturation polarization (J_S) and coercivity (H_C) as a function of the Cr content for $Co_{100-x}Cr_x$ ($10 < x < 90$, $\Delta x = 10$) milled for 7 h.

The coercivity behavior as a function of the chromium content is also shown in Fig. 5. A tendency to increase from 12.5 to 34 kA/m (157 to 435 Oe) for $Co_{90}Cr_{10}$ to $Co_{40}Cr_{60}$, respectively, is observed. Then it falls up to 21.6 kA/m (272 Oe) for compositions upwards of 90% of chromium. The magnetic hardening of the alloys manifested by the increasing of H_C values can be associated with the crystal size changes (Fig. 2) related to the reduction of the crystal diameter of the magnetic entities that promote the single domain state, for which noticeable H_C improvement has been reported in magnetic alloys [25]. Additionally, the increase of H_C can be a consequence of the allotropic transformation of Co, from fcc to hcp [16]. Conversely, the decreasing H_C tendency observed for $x > 60$ is a consequence of the larger crystal size, and possibly the change of crystalline structure, i.e., the obtaining of a cubic-bcc phase. The behavior of the H_C is because of the coercivity is an extrinsic property of magnetic materials, which strongly depends on the microstructure of the material including the effects of internal defects, residual stresses, grain sizes, and non-magnetic inclusions [26].

Moreover, the magnetic anisotropy constant was determined for each composition using the law of approach to saturation. According to this law, the magnetization, *M*, can be expressed as a function of the magnetic field, *H*, in the saturation region as follow [27]:

$$M = M_s\left(1 - \frac{a}{H} - \frac{b}{H^2}\right) \tag{2}$$

where M_s is the saturation magnetization, the term b/H^2 is caused by a uniform magnetocrystalline anisotropy, and a/H is attributed to the existence of structural defects and non-magnetic inclusions. The parameter *b* can be expressed in terms of the first order uniaxial magnetic anisotropy, K_1, as follows:

$$b = \frac{4K_1^2}{15M_S^2} \tag{3}$$

For the case of a ferromagnetic material with a cubic crystal structure, the coefficient *b* is given by Eq. (4):

$$b = \frac{8K_1^2}{105M_s^2} \tag{4}$$

where K_1 is the cubic first order anisotropy constant [27].

Fig. 6 displays the magnetocrystalline anisotropy, K_1, for the $Co_{100-x}Cr_x$ system. As can be observed, K_1 exhibits a decreasing behavior up to $x = 60$, followed by a recovery for the remaining Cr contents. This is a result of the phase evolution from the hcp to bcc crystal structures because the magnetocrystalline anisotropy of hcp-Co phase is considerably higher than that corresponding to the bcc-Co structures [28]. Cobalt exhibits two allotropic phases: ε-hcp and α-fcc. The hcp phase is stable at low temperatures, until 673 K, while fcc phase is stable from 673 K up to the melting point. This transformation depends on the impurity content, thermal treatments, grain size, and the number and type of imperfections that occur when cobalt is subjected to an external mechanical or thermal energy [3,14,17,19–22]. Besides, Co shows interesting magnetic properties associated to the allotropic phases, both phases show ferromagnetic behavior with different Curie temperature, T_C, which is a characteristic of each phase. The Curie temperature for α-fcc was quantified between 1367 and 1404 K by

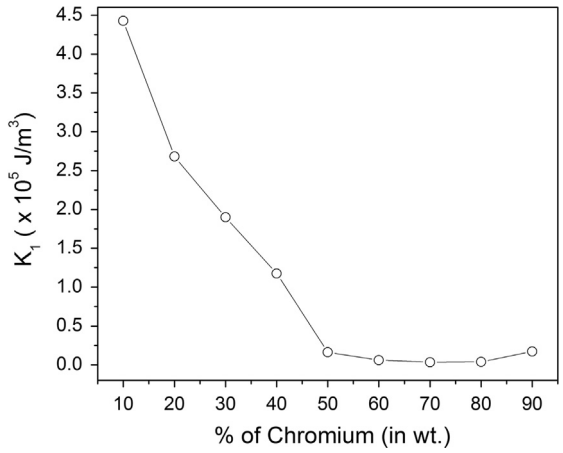

Fig. 6. Magnetocrystalline anisotropy constant, K_1, as a function of the Cr content, x, for the $Co_{100-x}Cr_x$ ($10 < x < 90$, $\Delta x = 10$) milled for 7 h.

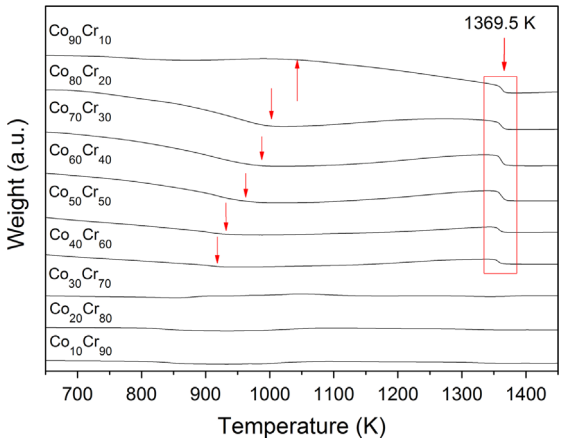

Fig. 7. Curie temperature for $Co_{100-x}Cr_x$ ($10 < x < 90$, $\Delta x = 10$) milled for 7 h.

Nishizawa et al. [29] and Ray et al. [30]. However, the T_C of the ε-hcp phase is not clear because direct measurements are difficult [29]. The Curie temperature of the hexagonal phase was estimated by extrapolating between 1130 K and 1170 [31,32].

In order to study the magnetic behavior of the studied system, the Curie temperatures for all the compositions $Co_{100-x}Cr_x$ were derived from magnetic thermogravimetric analysis shown in Fig. 7. As can be observed in this figure, two events at 1041 and 1369.5 K for the $Co_{90}Cr_{10}$ composition were detected. The first event at 1041 K can be associated with the Curie temperature of the hcp-Co(Cr) solid solution, and the second event at 1369.5 K (marked in the figure with a rectangle), can be attributed to the T_C of the fcc-Co(Cr) which is reported at 1400 K for fcc-Co, slightly higher than the value obtained. This diminishing is associated with the formation of the fcc-Co(Cr) solid solution. In both cases, the difference in temperature can be attributed to the effect of the MA process which can affect the interatomic bonding distance between cobalt atoms, thereby influencing the exchange coupling interaction and, therefore, the Curie temperature.

For all the compositions, the first magnetic thermogravimetric event (marked in the figure with arrows) confirms the incorporation of chromium atoms into the structure of cobalt to form a hcp-Co(Cr) solid solution. This incorporation promotes a reduction in the Curie temperature. Also, the decrease of the temperature is related to the increase of the Cr content for the next compositions.

The transition observed at 1369.5 K is only present for the compositions $Co_{100-x}Cr_x$ with x in the range from 10 to 60, and it is associated with the T_C of the fcc-Co(Cr) solid solution. However, Glagoleva et al. [33] reported lower values of this composition. This difference is associated with the synthesis method because the MA process modifies the properties of the materials obtained under non-equilibrium conditions [34]. In addition, the MA process leads to a considerable size reduction of the powders and a large amount of structural defects caused by severe plastic deformation [34,35], thereby causing noticeable changes in the magnetic properties [9]. The intensity of this magnetic event diminishes as the amount of chromium is increased, which confirms the inclusion of Co atoms into the chromium structure to form a different solid solution.

Finally, for $Co_{70}Cr_{30}$, $Co_{80}Cr_{20}$ and $Co_{10}Cr_{90}$ compositions, no thermal–magnetic events are observed. This suggests the complete incorporation of the cobalt atoms into the chromium structure, obtaining a bcc-Co(Cr) solid solution for these compositions which is fully consistent with the X-ray diffraction patterns shown in Fig. 1.

4. Conclusions

The XRD results confirm that an allotropic transformation of cobalt from fcc→hcp phase occurs along with the formation of hcp-Co(Cr) and fcc-Co(Cr) solid solutions for $Co_{90}Cr_{10}$ and $Co_{80}Cr_{20}$. For $Co_{10}Cr_{90}$, $Co_{20}Cr_{80}$ and $Co_{30}Cr_{70}$ a bcc-Cr(Co) solid solutions is obtained after 7 h of milling time by mechanical alloying method. The magnetic measurements indicate that the highest saturation polarization of 1.17 T (144 Am^2/kg) is obtained for the composition with the lowest chromium content ($Co_{90}Cr_{10}$), followed by the reduction with the increasing Cr concentration due to the dilution effect of the magnetic moment promoted by Cr. Furthermore, the coercivity was observed to be strongly dependent upon the crystal size and crystalline structure, reaching a maximum value of 34 kA/m (435 Oe) for $Co_{40}Cr_{60}$. The magnetic thermogravimetric analysis allowed to obtain Curie temperatures corresponding to fcc-Co(Cr) solid solutions at 1369.5 K, for $Co_{1-x}Cr$ with x from 10 to 60. Other thermal magnetic events attributed to hcp-Co(Cr) solid solution were also observed. For compositions from 70 to 90 wt% of Cr, there are not thermomagnetic events, which is due to the formation of the bcc-Cr(Co) phase.

Acknowledgements

This project was financially assisted by the National Science and Technology Council of Mexico, CONACyT from México under grant no. 129910 and 130413.

References

[1] K.H.J. Buschow, R.W. Cahn, M.C. Flemings, B. Ilschner, E.J. Kramer, S. Mahajan., The Science and Technology of Materials: An Introduction.Encyclopedia of Materials: Science and Technology, second ed., Elsevier (2009) http://dx.doi.org/10.1016/B0-08-043152-6/01863-5.
[2] R.W. Cahn, P. Haasen, E.J. Kramer, Materials science and technology, in: D. F. Williams (Ed.), Medical and Dental Materials, 14, VCH Verlag, Weinheim, 1992.
[3] S. Loudi, F.Z. Betayeb, W. Tebib, J.J. Suñol, A.M. Mercier, J.M. Grenéche, Amorphisation of Cr–10Co mixture by mechanical alloying, J. Non-Cryst. Solids 356 (2010) 1052–1056.
[4] P.J. Grundy, Thin film magnetic recording media, J. Phys. D: Appl. Phys. 31 (1998) 2975–2990.
[5] L.M. Di, H. Bakker, F.R. de Boer, Atomic disorder induced by mechanical milling in the intermetallic compound CoAl, Physica B 182 (1992) 91–98.
[6] F.C. Campbell, Cobalt and Cobalt Alloys, Elements of Metallurgy and Engineering Alloys, ASM International (2008) 557–558.
[7] M.A. García-Contreras, S.M. Fernández-Valverde, J.R. Vargas-García, Oxigen reduction on cobalt–nickel alloys prepared by mechanical alloying, J. Alloys Compd. 434–435 (2007) 522–524.
[8] C. Suryanarayana (Ed.), Mechanical Alloying and Milling, Marcel Dekker, New York, 2004.

[9] S. Louidi, F.Z. Bentayeb, W. Tebib, J.J. Suñol, L. Escoda, A.M. Mercier, Formation study of nanostructured $Cr_{100-x}Co_x$ ($x=10$, 90) alloys, J. Alloys Compd. 536 (2012) S365–S369.
[10] S. Louidi, F.Z. Bentayeb, W. Tebib, J.J. Suñol, L. Escoda, A.M. Mercier, Stacking faults and phase transformations study in ball milled $Co_{100-x}Cr_x$ ($x=0$, 20, 50) alloys, Mater. Chem. Phys. 132 (2012) 761–765.
[11] L.M. Kubalova, V.I. Fadeeva, I.A. Sviridov, Structural transformations in $Co_{87}B_{13}$ and $Ni_{87}B_{13}$ alloys during ball milling and influence of stacking faults in FCC Co on amorphous phase formation, Rev. Adv. Mater. Sci. 18 (2008) 360–365.
[12] F. Sánchez-De Jesús, A.M. Bolarin-Miro, G. Torres-Villaseñor, C.A. Cortés-Escobedo, J.A. Betancourt-Cantera, Mechanical alloying of biocompatible $Co_{28}Cr_6Mo$ alloy, J. Mater. Sci. - Mater. Med. 21 (2010) 2021–2026.
[13] J.Y. Huang, Y.K. Wu, H.Q. Ye, K. Lu, Allotropic transformation of cobalt induced by ball milling, NanoStruct. Mater. 6 (1995) 723–726.
[14] H. Moumeni, A. Nemamcha, S. Alleg, J.M. Grenéche, Stacking faults and structure analysis of ball-milled Fe–50%Co powders, Mater. Chem. Phys. 122 (2010) 439–443.
[15] F.Z. Bentayeb, S. Alleg, J.M. Grenéche, Structural and microstructural study of Fe–31Cr–12Co mixture prepared by ball milling, J. Alloys Compd. 434 (2007) 477–480.
[16] J. Sort, J. Nogués, S. Suriñach, J.S. Muñoz, M.D. Baró, Correlation between stacking fault formation, allotropic phase transformations and magnetic properties of ball-milled cobalt, Mater. Sci. Eng., A 375 (2004) 869–873.
[17] F. Cardellini, G. Mazzone, Thermal and structural study of the hcp to fcc transformation in cobalt, Philos. Mag. A 67 (1992) 1289–1300.
[18] S. Alleg, F.Z. Bentayeb, R. Bensalem, C. Djebbari, L. Bessais, J.M. Grenéche, Effect of the milling conditions on the formation of nanostructured Fe–Co powders, Phys. Status Solidi A 205 (2008) 1641–1646.
[19] J.A. Betancourt-Cantera, F.S.-D. Jesús, G. Torres-Villaseñor, A.M. Bolarín-Miró, C.A. Cortés-Escobedo, Extended solid solubility of a Co–Cr system by mechanical alloying, J. Alloys Compd. 529 (2012) 58–62.
[20] H. Shokrollanhi, The magnetic and structural properties of most important alloys of iron produced by mechanical alloying, Mater. Des. 30 (2009) 3374–3387.
[21] N. Loudjani, N. Bensebaa, L. Dekhil, S. Alleg, J.J. Suñol, Sturctural and magnetic properties of $Co_{50}Ni_{50}$ powders mixture, J. Magn. Magn. Mater. 323 (2011) 3063–3070.
[22] K. Akkouche, A. Guittoum, N. Boukherrroub, N. Souami, Evolution of structure, microstructure and hyperfine properties of nanocrystalline $Fe_{50}Co_{50}$ powders prepared by mechanical alloying, J. Magn. Magn. Mater. 323 (2011) 2542–2548.
[23] M. Khajepour, S. Sharafi, Characterization of nanostructured Fe–Co–Si powder alloy, Powder Technol. 232 (2012) 124–133.
[24] Z. Hua, Y.M. Sun, W.Q. Yu, M.B Wei, L.H. Liu, Structure and magnetic properties of $Fe_{88-x}Zr_xB_{12}$ ($x=5$, 10, 20) alloys prepared by mechanical alloying, J. Alloys Compd. 447 (2009) 529–531.
[25] M.J. Bonder, Y. Huang, G.C. Hadjipanayis, in: D. Sellmyer, R. Skomski (Eds.), Magnetic Nanoparticles in Advanced Magnetics NanostructuresSpringer, New York, 2010, pp. 183–206.
[26] A. Behvandi, H. Shokrollahi, B. Chitsazan, M. Ghaffari, Magnetic and structural studies of mechanical alloyed nanostructured $Fe_{49}Co_{49}V_2$ powders, J. Magn. Magn. Mater. 322 (2010) 3932–3937.
[27] S.V. Andreev, M.I. Bartashevich, V.I. Pushkarsky, V.N. Maltsev, L.A. Pamyatnykh, E. N. Tarasov, N.V. Kudrevatykh, T. Goto, Law of approach to saturation in highly anisotropic ferromagnets application to Nd–Fe–B melt-spun ribbons, J. Alloys Compd. 260 (1997) 196–200.
[28] S. Chikazumi, in: E. Robert (Ed.), Physics of Magnetism, Krieger Publishing Co, New York, 1978.
[29] T. Nishizawa, K. Ishida, The Co (Cobalt) system, Bull. Alloy Phase Diagram 4 (1983) 387–390.
[30] A.E. Ray, S.R. Smith, J.D. Scofield, Study of the phase transformation of cobalt, J. Phase Equilib. 12 (1991) 644–647.
[31] A.J.P. Meyer, P. Taglang, The magnetic moments and Curie points of hexagonal and cubic cobalt, C.R. Acad. Sci. 231 (1950) 612.
[32] W. Sucksmith, Magnetic saturation intensity and some other related measurements, J. Phys. Radium 12 (1951) 430.
[33] Yu.V. Glagoleva, V.F. Polev, V.I. Gorbatov, A.D. Ivliev, A.A. Kurichenco, S.G. Taluts, I.G. Korshunov, Thermal and kinetic properties of cobalt–chromium alloys at high temperatures, Phys. Met. Metall. 107 (2009) 254–261.
[34] S. Alleg, S. Azzaza, R. Bensalem, J.J. Suñol, S. Khene, G. Fillion, Magnetic and structural studies of mechanically alloyed $(Fe_{50}Co_{50})_{62}Nb_8B_{30}$ powders mixture, J. Alloys Compd. 482 (2009) 86–89.
[35] A.M. Bolarin-Miró, F. Sánchez-De Jesús, G. Torres-Villaseñor, C.A. Cortés-Escobedo, J.A. Betancourt-Cantera, J.I. Betancourt-Reyes, Amorphization of Co-base alloy by mechanical alloying, J. Non-Cryst. Solids 357 (2011) 1705–1709.